Continuous Fermi level tuning of Nb-doped WSe_2 under an external electric field

Kaoru Hisama[1]*, Yanlin Gao[1] Mina Maruyama[1], Ryo Kitaura[2], and Susumu Okada[1]

[1]*Department of Physics, University of Tsukuba, Tsukuba 305-8571, Japan*

[2]*Department of Chemistry, Nagoya University, Nagoya 464-8602, Japan*

The possibility of continuous Fermi level tuning of Nb-doped WSe_2 under an external electric field is investigated, using the density functional theory combined with the effective screening medium method. The Fermi level monotonically increases and decreases as the carrier concentration increases and decreases, respectively, by controlling the external electric field. The electronic structure of Nb-doped WSe_2 is insensitive to the Nb concentration and arrangement. Furthermore it was demonstrated that the electric field simply shifts the Fermi level of Nb-doped WSe_2, resulting in the constant quantum capacitance through the gate voltage, irrespective of the Nb concentration and arrangement.

1. INTRODUCTION

Transition metal dichalcogenides (TMDCs), such as MoS_2 [1, 2], $MoSe_2$ [3], WS_2 [4], WSe_2 [5], and $MoTe_2$ [6], are representative examples of atomic layer materials [7]. These materials have a hexagonal covalent network with a thickness of approximately 3 Å, comprising an atomic layer of transition metals that form a triangular lattice sandwiched by atomic layers of chalcogens arranged in prismatically. Hexagonal covalent networks comprising transition metals and chalcogens cause chemically inert surfaces by their tight covalent networks, allowing them to form layered structures, each of which is bound by a weak van der Waals interaction [8]. Due to the chemical valence of constituent elements and van der Waals interactions, most TMDCs are semiconductors whose electronic structure strongly depends on the constituent elements and the number of layers [9, 10]. Furthermore, van der Waals interlayer interaction allows the tailoring of heterolayered structures by layer-by-layer stacking of TMDCs [11, 12]. Such heterostructures exhibit further varying electronic structures near the band edges due to the relative band edge alignment of constituent TMDC layers. Most of the bilayer heterostructures of TMDCs are Type II semiconductors [13–18], whereas MoS_2/ReS_2 and $MoTe_2/WSe_2$ heterostructures are Type I semiconductors owing to the large band edge

*E-mail: khisama@comas-tsukuba.ac.jp

offset between constituent layers [19, 20].

The tunable band edge alignments and atomic layer structure of TMDCs make them emerging materials for designing field-effect transistors (FETs), with the few-atomic thicknesses which are applicable for flexible electronics [21], photonics [22] and optoelectronics [23]. Precisely, most monolayer TMDCs are intrinsic semiconductors with a direct band gap at the K point, so that these monolayer TMDCs on appropriate supporting substrates can work as a conducting channel of FETs with ultimately thin thickness [24]. Additionally, due to the intrinsic semiconducting property of pristine TMDCs, TMDCs also act as n- and p-type semiconductors by implanted appropriate dopant atoms [25–27]. In such doped semiconducting TMDCs, Nb and Re are possible dopant atoms for providing p- and n-type properties of doped TMDCs [28]. Indeed, the Nb atoms implanted into WSe_2 cause holes in the valence band of WSe_2 without substantial modification of the electronic band structure of the host WSe_2. In addition to the intrinsic carrier doping by atomic dopants, further carrier density control is required to apply the TMDCs for switching devices.

This study aims to explore the possibility of continuous Fermi level tuning of Nb-doped WSe_2 by the external electric field using density functional theory (DFT) combined with the effective screening medium method (ESM). The calculation results revealed that the Fermi level of Nb-doped WSe_2 monotonically increases and decreases as the gate voltages increase and decrease up to ± 2.1 V, respectively, irrespective of the Nb density and arrangements. Thus, the gate voltage continuously controls the hole density in WSe_2. Furthermore, it was elucidated that the electronic structures of Nb-doped WSe_2 are insensitive to the Nb arrangement and gate voltages, resulting in the constant quantum capacitance through the gate voltages studied herein. These results indecate that Nb-doped WSe_2 is a promising p-channel material for FET where the gate electric field continuously tunes the Fermi level.

2. METHODS AND MODELS

DFT [29, 30] was implemented in the Simulation Tool for Atom Technology (STATE) package [31], to perform all calculations herein. The general gradient approximation (GGA) with the Perdew-Burke-Ernzerhof (PBE) functional [32, 33] was applied to express the exchange-correlation potential energy among interacting electrons. The interactions between the valence electrons and the nuclei were provided by the ultrasoft pseudopotential generated by the Vanderbilt scheme [34]. Wavefunctions and deficit charge density were expanded by plane-wave basis set with the cutoff energy of 25 and 225 Ry, respectively. To simulate the Nb-doped WS_2 implemented in the FET structure, the structural model shown in Figure 1 was

considered, where the Nb-doped WS_2 is located below the planar metal electrode with a 7-Å vacuum spacing. The electrode was simulated by an effective screening medium with infinite dielectric constant, which control the carrier densities in Nb-doped WSe_2 by solving the generalized Poisson equation in the form of the ESM [35]. To investigate the effect of the dopant density and arrangements, 6×6 lateral supercell were considered in which one or two Nb atoms were substitutionally doped. Six possible mutual Nb arrangements in WSe_2 were considered [Figs. 1(b) – (h)] for the case with 5.54% Nb-doping concentration. The arrangement I is the most stable one among six Nb arrangements. The relative total energy gradually increases with increase of the Nb-Nb spacing by 90 meV. In addition to the Nb-Nb spacing, the energy clearly depend on mutual Nb arrangements: The mutual arrangements along armchair direction has lower energy than those along zigzag direction [Fig. 1(i)]. The Brillouin-zone integration was performed with the 2×2×1 $\vec{k}$-meshes for self-consistent electronic structure calculations, which correspond with 12×12×1 $\vec{k}$-meshes of monolayer WSe_2 with the primitive 1×1 cell. All atoms were fully optimized under zero electric field until the remaining force acting on each atom was less than 0.005 Ry/Å under the fixed lateral lattice parameter a=19.68Å, which corresponds to the experimental value. Atomic coordinates are fixed to those obtained under the zero electric field during the electronic structure calculations under the electric field. It should be noted that the force acting on each atom under the highest electric field is 0.02 Ry/AA which may cause the small but further structural relaxation on WSe_2.

3. RESULTS AND DISCUSSION

The Fermi level energy of Nb-doped WSe_2 monotonically increases as the gate voltage increases from -2.1 to 2.1 V without displaying any plateaus [Figs. 2(a) – (g)]. Therefore, the gate voltage continuously controls the Fermi level energy of Nb-doped WSe_2, indicating that it works as a p-type channel of a TMDC-FET. The Fermi level energy as a function of the gate voltage is almost insensitive to the mutual Nb arrangement, except the Nb concentration of 2.77% and 5.54% with arrangement I. This trend implies that the electronic structure of Nb doped WSe_2 is insensitive to the Nb arrangement. Thus, the density of states (DOS) of Nb-doped WSe_2 with the Nb concentration of 5.54% has similar structures around the Fermi level energy [Figs. 3(a) – (g)]. Furthermore, the DOS approximately retains the spectral shape around the Fermi level under the finite gate voltages, indicating that the rigid band picture is applicable for discussing the physics under low carrier concentration in the valence band edge. The rigid band, which appears irrespective of Nb arrangement and gate voltage, also

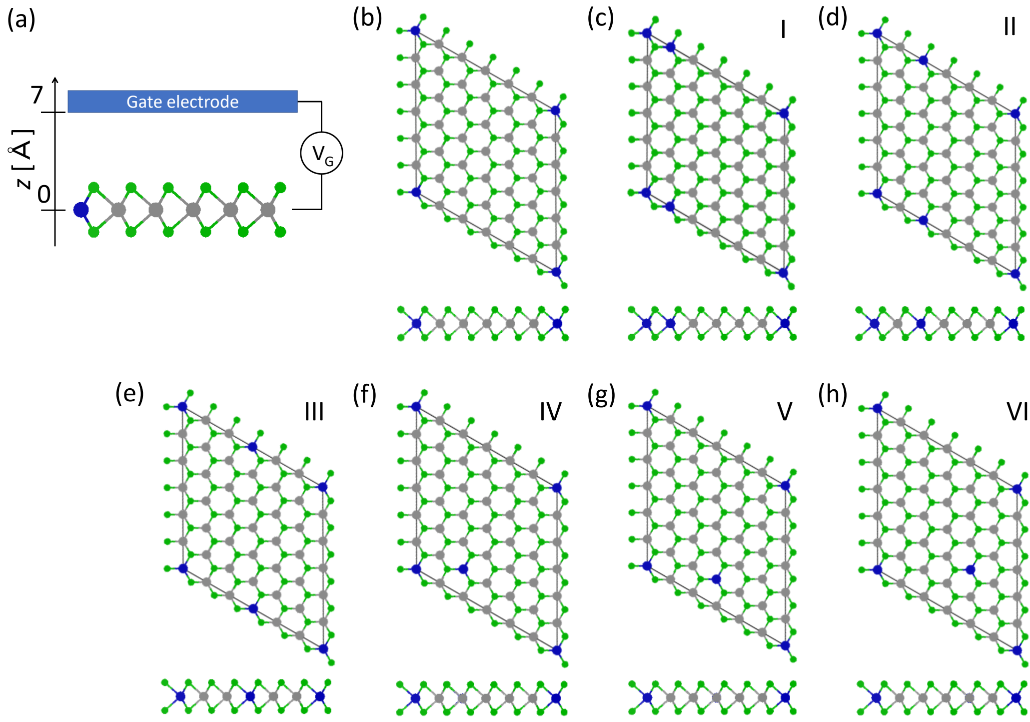

Fig. 1. (a) Structural model of Nb-doped WSe_2 FET. Blue-shaded rectangle indicates the counter electrode simulated by an effective screening medium with the infinite dielectric constant. (b) Optimized structure of Nb-doped WSe_2 with 2.77% Nb-doping concentration. Optimized structures of Nb-doped WSe_2 with 5.54% Nb-doping concentration and mutual Nb arrangements of (c) I, (d) II, (e) III, (f) IV, (g) V, and (h) VI. Blue, gray, and green filled circles denote Nb, W, and Se atoms, respectively. Blue, gray, and green filled circles denote Nb, W, and Se atoms, respectively. Relative total energy of Nb-doped WSe_2 with the doping concentration of 5.54 % as a function of Nb-Nb spacing. The energies are measured from that of the Nb arrangement I.

implies that any localized states associated with the dopant are absent near the valence band edge.

Continuous Fermi level energy tuning by the external electric field implies that the carrier is also continuously injected into Nb-doped WSe_2 in terms of the electric field and is extended through the WSe_2. Carriers injected by the gate voltage are primarily distributed on Se atomic sites located at the electrode side and extended through the surface irrespective of the carrier density and species [Figs. 4(a) – (g)]. Accumulated carrier density with respect to the electrode is evaluated using

$$\Delta\rho(z) = \int dxdy(\rho_V(\vec{r}) - \rho_0(\vec{r}))$$

where $\rho_V(\vec{r})$ and $\rho_0(\vec{r})$ indicate valence charge density of Nb-doped WSe_2 with and without the gate voltage, respectively. Besides the primary carrier distribution on the topmost Se layer,

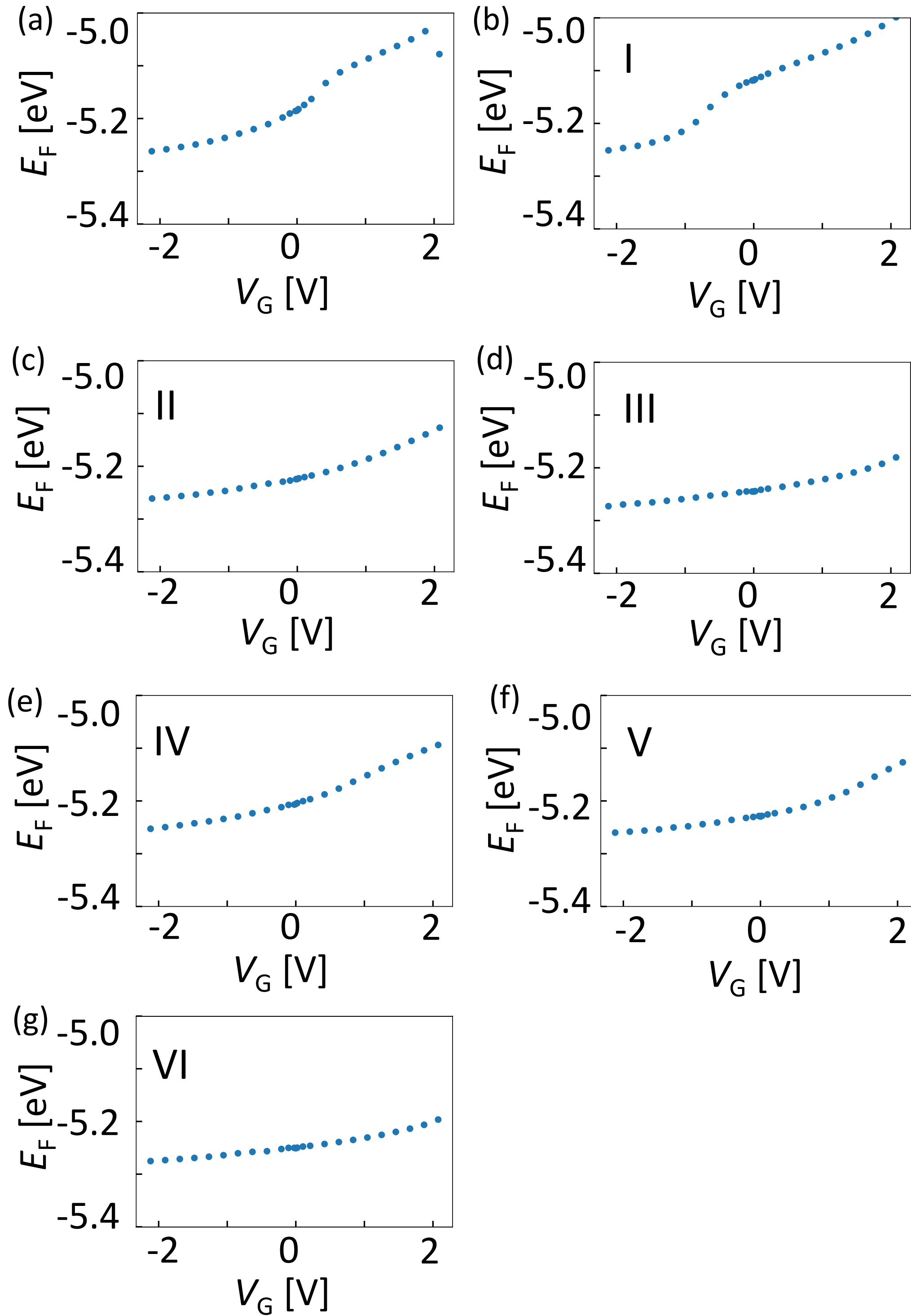

Fig. 2. (a) Fermi level energy as a function of gate voltage of Nb-doped WSe_2 with 2.77% Nb-doping concentration. Fermi level energy as a function of gate voltage of Nb-doped WSe_2 with 5.54% Nb doping concentration and mutual Nb arrangements of (b) I, (c) II, (d) III, (e) IV, (f) V, and (g) VI.

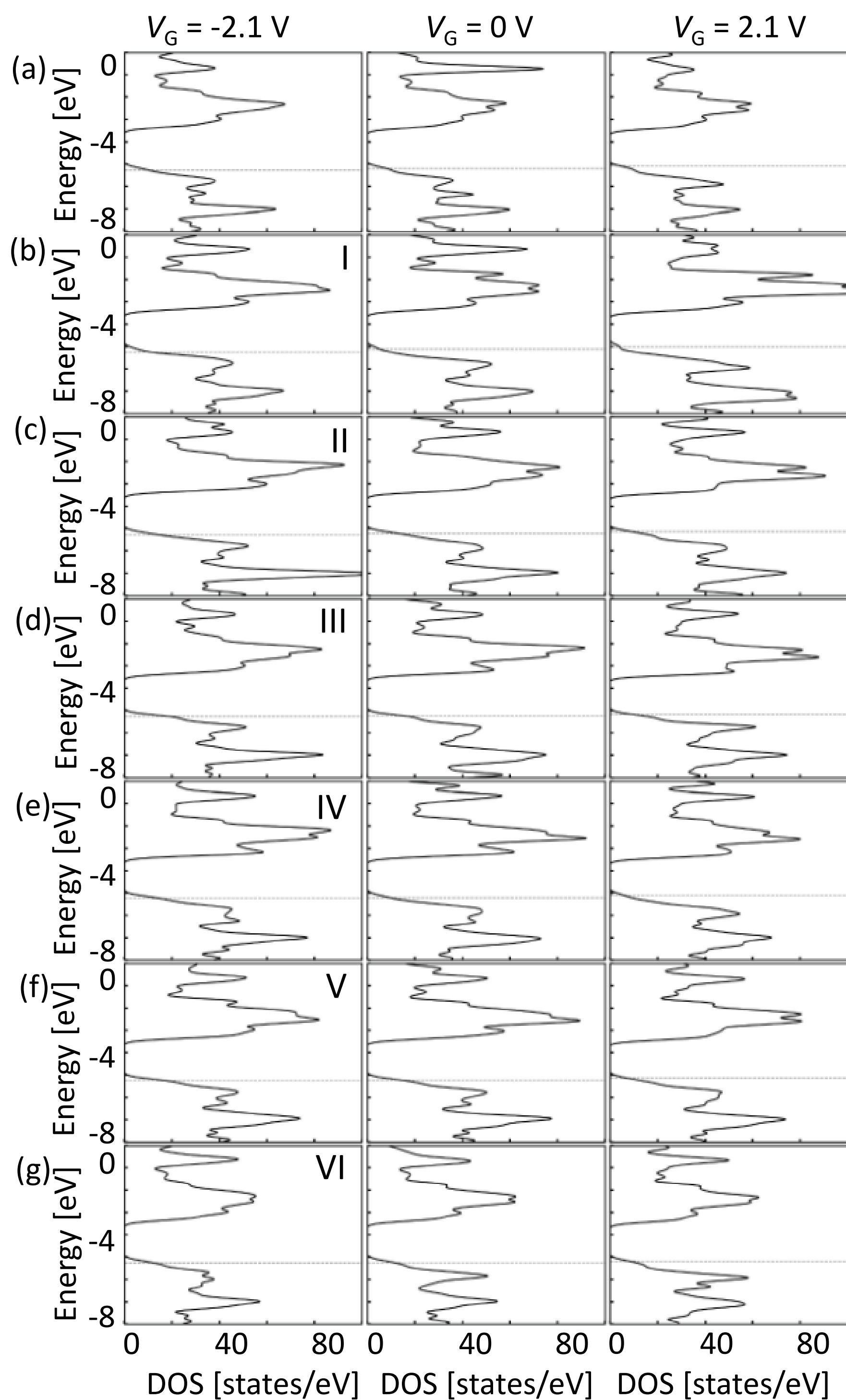

Fig. 3. (a) DOS of Nb-doped WSe_2 with 2.77% Nb-doping concentration. DOS of Nb-doped WSe_2 with 5.54 Nb-doping concentration and mutual Nb arrangements of (b) I, (c) II, (d) III, (e) IV, (f) V, and (g) VI.

the injected carriers are also substantially distributed on the W layer. In the W atomic layer, contour plot of accumulated carrier,

$$\Delta\rho(\vec{r}) = \rho_V(\vec{r}) - \rho_0(\vec{r}),$$

is extended through the layer, but slightly concentrated at W atoms adjacent to Nb atoms. The substantial carrier penetration in the W layer may decrease the quantum capacitance of Nb-doped WSe_2 than that of an ideal parallel gate capacitor. The distribution of accumulated carriers normal to the WSe_2 layer is insensitive to the Nb concentration and arrangements, resulting in insesitivity of the capacitance to Nb arrangements. The approximately uniform distribution of carrier through the topmost Se layer also implies that Nb and gate voltage basically do not affect the transport properties of valence band edge of WSe_2. Detail carrier distribution around around Nb in W layer may cause the structure around the Fermi level for Nb-doped WSe_2 with 2.77% and 5.54% doping concentration with mutual arrangement I. For these structures, accumulated carriers is slightly localized around the Nb atoms, which is different from the carrier density for other Nb arrangements.

Figures 5(a)–(g) show the quantum capacitance of Nb-doped WSe_2 as a function of the gate voltages. In these calculations, the carrier density value is controlled by the counter electrode ranging from -2.98×10^{13} e/cm^2 (hole doping) to 2.98×10^{13} e/cm^2 (electron doping), which approximately corresponds with the gate voltages ranging from -2.1 to 2.1 V, respectively. The calculated capacitance is ~0.023 aF/nm^2 throughout the gate voltage, which is insensitive to the Nb density and arrangement. The capacitance is larger than that with the parallel metal electrodes located at the Se layer position by 0.007 aF/nm^2. The larger capacitance is attributed to the peak position of the accumulated carriers. The carriers are mainly distributed in the vacuum space outside the atomic positions of the WSe_2 layer. Moreover, as delineated above, the carrier distribution shape is approximately proportional to the gate voltage or carrier concentration, reflecting the constant capacitance through the gate voltage.

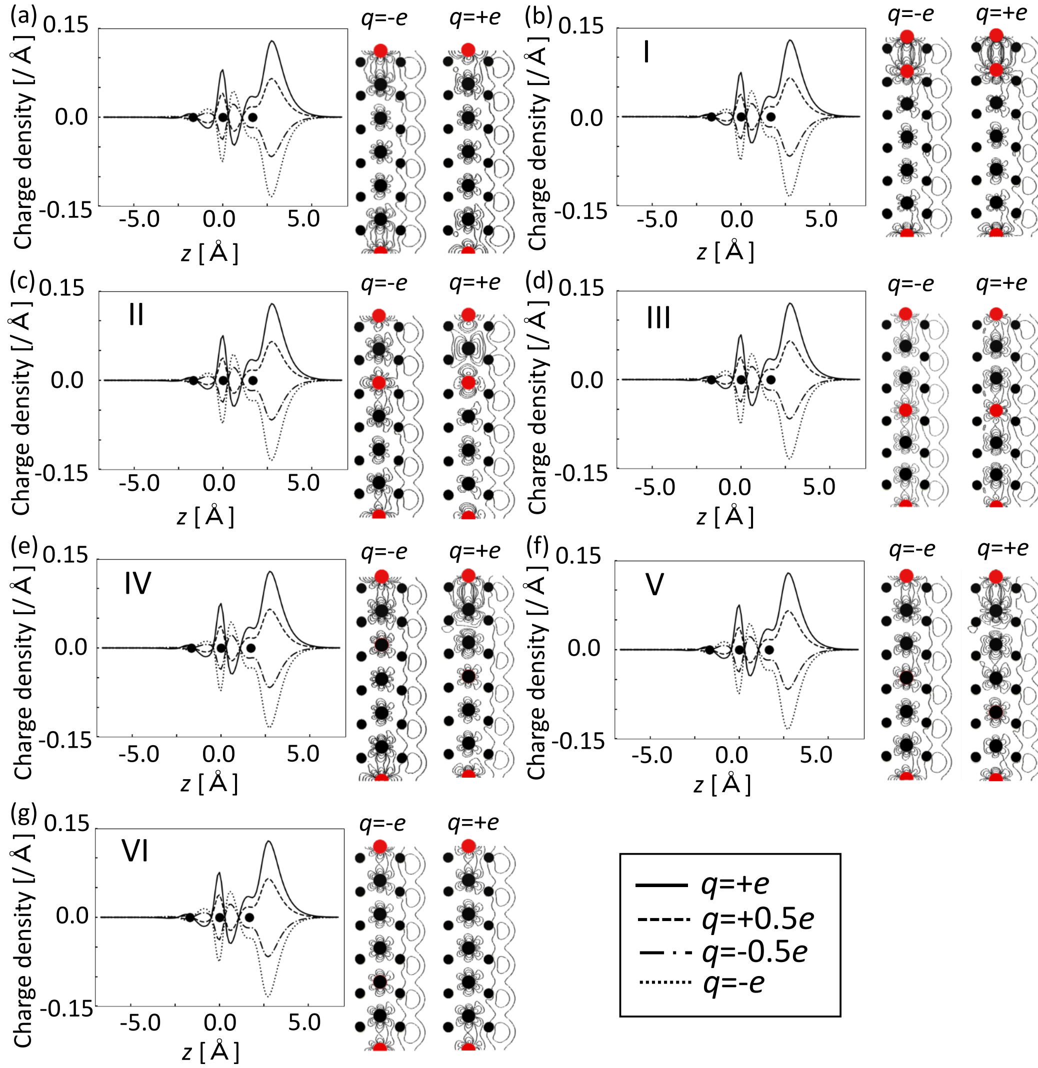

Fig. 4. (a) Plane integrated accumulated carrier distribution across layer ($\Delta\rho(z)$) and contour plots of accumulated carrier ($\Delta\rho(\vec{r})$ under the gate voltages ±2.1 V with 2.77% Nb-doping concentration. Accumulated carrier distribution across layer and contour plots of carrier under gate voltages ±2.1 V with 5.54% Nb-doping concentration and mutual Nb arrangements of (b) I, (c) II, (d) III, (e) IV, (f) V, and (g) VI. Contours are depicted on $(10\bar{1}0)$ plane where contains Nb atoms located at the origin. Filled red and black circles denote atomic positions of Nb and other atoms, respectively.

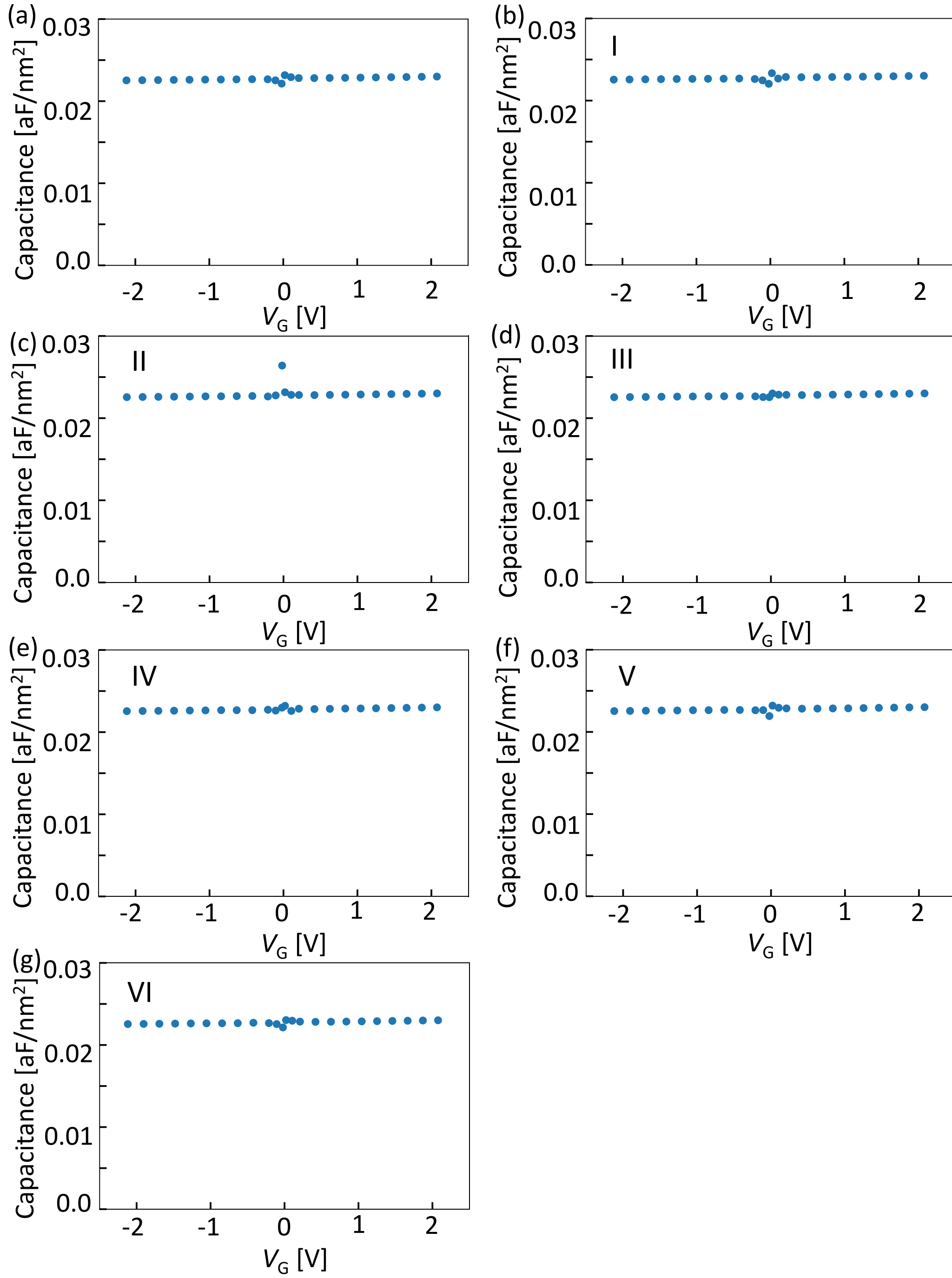

Fig. 5. (a) Quantum capacitance of Nb-doped WSe_2 with 2.77% Nb-doping concentration. Quantum capacitances of Nb-doped WSe_2 with 5.54% Nb-doping concentration and mutual Nb arrangements of (b) I, (c) II, (d) III, (e) IV, (f) V, and (g) VI.

4. CONCLUSION

Based on DFT, combined with the ESM, the electronic structure of Nb-doped WSe_2 under an external electric field was calculated in terms of the Nb concentration and arrangement. The Fermi level energy monotonically increases as the gate voltage increases, indicating that the Fermi level of Nb-doped WSe_2 in FET is continuously controlled by the external field, irrespective of the Nb concentration and mutual arrangement. Therefore, the Nb-doped WSe_2 is a possible p-channel material for gate-controlled switching devices. The calculated quantum capacitance of Nb-doped WSe_2 with planar gate electrode possesses a 0.023 aF/nm^2 constant value through the gate voltage studied herein. Furthermore, the capacitance is also insensitive to the Nb concentration and arrangement. Due to the constant capacitance, the distribution of the accumulated carriers by the gate voltage exhibits similar characteristics for all Nb concentrations and arrangements. The carriers are primarily distributed on the topmost Se layer situated at the electrode side and substantially penetrated in the W atomic layer. In contrast to the distribution across the WSe_2 layer, the carriers almost uniformly extended through the WSe_2 layer. The doped Nb atom slightly augments the carrier density at W atomic site adjacent to the Nb atom. Besides, the electronic structure of Nb-doped WSe_2 is insensitive to the Nb concentration and arrangement, and is robust to the carrier injections.

Acknowledgement

The authors thank the Japan Science and Technology Agency, Core Research for Evolutionary Science and Technology (JST-CREST; Grant Nos. JPMJCR1715 and JPMJCR20B5) and the Japan Society for the Promotion of Science, Grants-in-Aid for Scientific Research (JSPS KAKENHI; Grant Nos. JP21H05233, JP21H05232, JP21K14484, JP20K22323, JP20H00316, JP20H02080, JP20K05253, and JP20H05664), the Joint Research Program on Zero-Emission Energy Research, Institute of Advanced Energy, Kyoto University, and the University of Tsukuba Basic Research Support Program (S). Part of the calculations was performed on an NEC SX-Ace and SQUID at the Cybermedia Center at Osaka University. Geometric structure and contour plots of charge density are depicted with the VESTA software [36].

References

1) K. F. Mak, C. Lee, J. Hone, J. Shan, and T. F. Heinz, Phys. Rev. Lett. **105**, 136805 (2010).
2) A. Splendiani, L. Sun, Y. Zhang, T. Li, J. Kim, C. Y. Chim, G. Galli, and F. Wang, Nano Lett. **10**, 1271 (2010).
3) X. Lu, M. I. B. Utama, J. Lin, X. Gong, J. Zhang, Y. Zhao, S. T. Pantelides, J. Wang, Z. Dong, Z. Liu, W. Zhou, and Q. Xiong, Nano Lett. **14**, 2419 (2014).
4) A. L. Elías, N. Perea-Lépez, A. Castro-Beltran, A. Berkdemir, R. Lv, S. Feng, A. D. Long, T. Hayashi, Y. A. Kim, M. Endo, H. R. Gutiérrez, N. R. Pradhan, L. Balicas, T. E. Mallouk, F. López-Urias, H. Terrones, and M. Terrones, ACS Nano **7**, 5235 (2013).
5) J.-K. Huang, J. Pu, C.-L. Hsu, M.-H. Chiu, Z.-Y. Juang, Y.-H. Chang, W.-H. Chang, Y. Iwasa, T. Takenobu, and L.-J. Li, ACS Nano **8**, 923 (2014).
6) J. C. Park, S. J. Yun, H. Kim, J.-H. Park, S. H. Chae, S.-J. An, J.-G. Kim, S. M. Kim, K. K. Kim, and Y. H. Lee, ACS Nano **9**, 6548 (2015).
7) J. Zhou, J. Lin, X. Huang, Y. Zhou, Y. Chen, J. Xia, H. Wang, Y. Xie, H. Yu, J. Lei, D. Wu, F. Liu, Q. Fu, Q. Zeng, C.-H. Hsu, C. Yang, L. Lu, T. Yu, Z. Shen, H. Lin, B. I. Yakobson, Q. Liu, K. Suenaga, G. Liu, and Z. Liu, Nature **556**, 355 (2018).
8) R. Friend and A. Yoffe, Adv. Phys. **36**, 1 (1987).
9) C. Gong, H. Zhang, W. Wang, L. Colombo, R. M. Wallace, and K. Cho, Appl. Phys. Lett. **103**, 053513 (2013).
10) R. Roldán, J. A. Silva-Guillén, M. P. López-Sancho, F. Guinea, E. Cappelluti, and P. Ordejón, Ann. Phys. **526**, 347 (2014).
11) A. K. Geim and I. V. Grigorieva, Nature **499**, 419 (2013).
12) M. Onodera, S. Masubuchi, R. Moriya, and T. Machida, Jpn. J. Appl. Phys. **59**, 010101 (2020).
13) C. H. Lee, G. H. Lee, A. M. Van Der Zande, W. Chen, Y. Li, M. Han, X. Cui, G. Arefe, C. Nuckolls, T. F. Heinz, J. Guo, J. Hone, and P. Kim, Nat. Nanotechnol. **9**, 676 (2014).
14) K. Wang, B. Huang, M. Tian, F. Ceballos, M.-W. Lin, M. Mahjouri-Samani, A. Boulesbaa, A. A. Puretzky, C. M. Rouleau, M. Yoon, H. Zhao, K. Xiao, G. Duscher, and D. B. Geohegan, ACS Nano **10**, 6612 (2016).
15) P. Rivera, J. R. Schaibley, A. M. Jones, J. S. Ross, S. Wu, G. Aivazian, P. Klement, K. Seyler, G. Clark, N. J. Ghimire, J. Yan, D. G. Mandrus, W. Yao, and X. Xu, Nat. Commun. **6**, 6242 (2015).

16) K. Zhang, T. Zhang, G. Cheng, T. Li, S. Wang, W. Wei, X. Zhou, W. Yu, Y. Sun, P. Wang, D. Zhang, C. Zeng, X. Wang, W. Hu, H. J. Fan, G. Shen, X. Chen, X. Duan, K. Chang, and N. Dai, ACS Nano **10**, 3852 (2016).

17) D. Kozawa, A. Carvalho, I. Verzhbitskiy, F. Giustiniano, Y. Miyauchi, S. Mouri, A. H. Castro Neto, K. Matsuda, and G. Eda, Nano Lett. **16**, 4087 (2016).

18) S. Mouri, W. Zhang, D. Kozawa, Y. Miyauchi, G. Eda, and K. Matsuda, Nanoscale **9**, 6674 (2017).

19) M. Z. Bellus, M. Li, S. D. Lane, F. Ceballos, Q. Cui, X. C. Zeng, and H. Zhao, Nanoscale Horiz. **2**, 31 (2017).

20) T. Yamaoka, H. E. Lim, S. Koirala, X. Wang, K. Shinokita, M. Maruyama, S. Okada, Y. Miyauchi, and K. Matsuda, Adv. Funct. Mater. **28**, 1801021 (2018).

21) D. Akinwande, N. Petrone, and J. Hone, Nat. Commun. **5**, 5678 (2014).

22) K. F. Mak and J. Shan, Nat. Photonics **10**, 216 (2016).

23) Q. H. Wang, K. Kalantar-Zadeh, A. Kis, J. N. Coleman, and M. S. Strano, Nat. Nanotechnol. **7**, 699 (2012).

24) M. Chhowalla, D. Jena, and H. Zhang, Nat. Rev. Mater. **1**, 16052 (2016).

25) L. Loh, Z. Zhang, M. Bosman, and G. Eda, Nano Res. **14**, 1668 (2021).

26) B. Schuler, J.-H. Lee, C. Kastl, K. A. Cochrane, C. T. Chen, S. Refaely-Abramson, S. Yuan, E. van Veen, R. Roldan, N. J. Borys, R. J. Koch, S. Aloni, A. M. Schwartzberg, D. F. Ogletree, J. B. Neaton, and A. Weber-Bargioni, ACS Nano **13**, 10520 (2019).

27) S. K. Pandey, H. Alsalman, J. G. Azadani, N. Izquierdo, T. Low, and S. A. Campbell, Nanoscale **10**, 21374 (2018).

28) K. Dolui, I. Rungger, C. Das Pemmaraju, and S. Sanvito, Phys. Rev. B **88**, 075420 (2013).

29) W. Kohn and L. J. Sham, Phys. Rev. **140**, A1133 (1965).

30) P. Hohenberg and W. Kohn, Phys. Rev. **136**, B864 (1964).

31) Y. Morikawa, K. Iwata, and K. Terakura, Appl. Surf. Sci. **169-170**, 11 (2001).

32) J. Perdew, K. Burke, and M. Ernzerhof, Phys. Rev. Lett. **77**, 3865 (1996).

33) J. P. Perdew, K. Burke, and M. Ernzerhof, Phys. Rev. Lett. **78**, 1396 (1997).

34) D. Vanderbilt, Phys. Rev. B **41**, 7892 (1990).

35) M. Otani and O. Sugino, Phys. Rev. B **73**, 115407 (2006).

36) K. Momma and F. Izumi, J. Appl. Crystallogr. **44**, 1272 (2011).